A Universal Scaling Collapse for Wiedemann–Franz Violations in Hydrodynamic Quantum Materials:

An Empirical Test of the SUI Framework

Michael Zot
ZotBot Research Initiative
Mike@zotbot.ai
ORCID: 0009-0001-9194-938X

December 10, 2025

Abstract. The Wiedemann–Franz (WF) law ties electrical conductivity and thermal conductivity in ordinary metals through a universal Lorenz number. Recent experiments on ultra-clean graphene and other hydrodynamic quantum materials report pronounced and robust violations of this law, suggesting a qualitatively new regime of electron transport. In parallel work, the SUI/LUI framework models intelligent and adaptive systems as evolving through discrete, thresholded update events called Smallest Units of Intelligence (SUIs), with macroscopic structures called Largest Units of Intelligence (LUIs) emerging from their accumulation.
This paper connects these two fronts. First, we introduce a concrete, parameter-light scaling procedure that maps the Lorenz ratio data of diverse hydrodynamic materials to a common, dimensionless frame. Second, we show how the SUI framework predicts a universal dome-shaped geometry for WF violations once each material is rescaled by its hydrodynamic temperature width and violation amplitude. Third, we test this universal dome hypothesis against existing datasets on graphene, WP_2, and WTe_2, and quantify the quality of collapse using residual statistics and bootstrap confidence intervals. Fourth, we compare the observed scaling structure to conventional quantum critical scaling and formulate a renormalization group style justification for the dome geometry.
The result is an explicit and falsifiable bridge between an abstract theory of discrete update events and concrete transport measurements in quantum materials. Either hydrodynamic electrons across distinct compounds share a common SUI-defined LUI class, or the scaling procedure fails and the SUI prediction is refuted in this domain. Both outcomes increase the signal-to-noise ratio of future work on hydrodynamic transport and discrete update laws.

1 Introduction

The Wiedemann–Franz law relates thermal conductivity κ and electrical conductivity σ in metals through the Lorenz number

$$L(T) = \frac{\kappa(T)}{\sigma(T)\,T}. \tag{1}$$

In ordinary Fermi liquids this ratio approaches a universal constant L_0 at low temperature, a result that has survived more than a century of experimental and theoretical scrutiny (Sommerfeld and Frank, 1911).

Hydrodynamic quantum materials present a sharp challenge to this picture. In ultra-clean graphene near its charge neutrality point, Crossno and collaborators observed a Dirac fluid regime in which the Lorenz ratio exceeds L_0 by nearly an order of magnitude (Crossno et al., 2016). In transition metal pnictides and dichalcogenides such as WP_2 and WTe_2, the Lorenz ratio falls well below L_0 at intermediate temperatures before recovering toward unity at low and high temperatures (Gooth et al., 2018; Xie et al., 2020). These systems realize an electron fluid that is neither a standard Fermi liquid nor a simple insulator, and their transport properties demand new organizing principles.

In parallel to these developments, the SUI/LUI framework was proposed as a unifying model of discrete update dynamics in adaptive systems (Zot, 2025). In that framework, a system accumulates prediction error or tension until a threshold is reached. At that threshold, an irreversible Smallest Unit of Intelligence (SUI) event occurs and the internal configuration jumps to a new basin. Aggregates of SUIs yield stable macrostructures called

Largest Units of Intelligence (LUIs). That work provided mathematical axioms, cross-domain predictions, and empirical tests in cognitive, neural, and chaotic physical systems.

The present paper asks a specific and concrete question. Can the SUI framework make a falsifiable prediction about electron hydrodynamics, in particular about the shape and universality of WF law violations in hydrodynamic quantum materials, and can this prediction be tested using existing data sets?

1.1 Aim of this paper

We focus on one sharp and tractable object: the temperature dependence of the normalized Lorenz ratio

$$\Lambda(T) \equiv \frac{L(T)}{L_0}. \tag{2}$$

In hydrodynamic materials, $\Lambda(T)$ exhibits a characteristic dome-shaped deviation from unity: it begins near one at low temperature, deviates strongly from one in an intermediate range where hydrodynamics dominates, and relaxes back toward one at high temperature where ordinary scattering processes recover control.

Our central goal is to introduce a scaling transformation that:

1. extracts a hydrodynamic center temperature T_{ext} and width scale ΔT_h from each material,
2. normalizes the Lorenz ratio deviation by its maximal amplitude,
3. and tests whether the resulting dimensionless curves collapse to a single universal dome.

The scaling procedure is guided by the SUI framework. Under SUI dynamics, hydrodynamic transport regimes are interpreted as LUIs built from SUIs that carry charge and heat through overlapping or distinct channels. WF validity corresponds to coincident SUIs for charge and heat; WF violation corresponds to a separation of these channels. If different materials share the same underlying SUI-controlled crossover between these regimes, their Lorenz ratio curves should become identical after appropriate rescaling. If they do not, the SUI universality claim fails for this class of systems.

1.2 Conceptual structure

The paper proceeds as follows.

Section 2 reviews the classical WF law and gives a concise summary of the SUI interpretation of hydrodynamic transport. Section 3 defines the scaling procedure in detail, including the hydrodynamic center and width and the dimensionless variables used for collapse. Section 4 formulates the universal dome hypothesis as a precise statement with associated theorems and lemmas under the SUI assumptions.

Section 5 applies the scaling procedure to data on graphene, WP_2, and WTe_2, using approximate reconstructions from published figures. We quantify the quality of collapse using residuals and a bootstrap error analysis described in Section 6. Section 7 compares the observed scaling to familiar quantum critical scaling forms and presents a renormalization group style justification for the dome geometry.

Section 9 tests the scaling on synthetic data generated from known functional forms to calibrate interpretation. Section 10 summarizes predictions and falsification conditions. Section 11 and Section 12 discuss implications and outline future measurements that could decisively support or refute the proposed universality.

Appendix A provides Python code for reproducing the scaling and plots. Additional technical details, including alternative fit functions and extended error analyses, appear in further appendices.

2 Background: WF law and SUI interpretation

2.1 The Wiedemann–Franz law

In a simple metal, the same quasiparticles that carry charge also carry energy. Under Fermi liquid assumptions and elastic scattering, one finds that the ratio of thermal to electrical conductivity satisfies

$$\frac{\kappa}{\sigma T} = L_0 = \frac{\pi^2}{3}\left(\frac{k_B}{e}\right)^2, \tag{3}$$

independent of microscopic details (Sommerfeld and Frank, 1911). Deviations from L_0 can occur at high temperatures, in the presence of inelastic scattering, or if longitudinal and transverse transport channels decouple. In most conventional metals these deviations are modest and restricted in range.

Hydrodynamic electron systems depart radically from this picture. In graphene near charge neutrality, strong electron-electron scattering enforces local equilibrium faster than momentum relaxing processes, leading to a collective Dirac fluid (Crossno et al., 2016). Experiments show a pronounced enhancement of κ relative to σ in this regime, with $\Lambda(T) \equiv L(T)/L_0$ significantly greater than one. In WP_2 and WTe_2, momentum conserving

normal scattering and strong Fermi surface anisotropy produce a very different hydrodynamic behavior where the Lorenz ratio falls below one (Gooth et al., 2018; Xie et al., 2020).

Although the microscopic mechanisms differ, a shared qualitative feature emerges. Each material has a low temperature regime where WF holds approximately, an intermediate hydrodynamic regime where WF is strongly violated, and a high temperature regime where inelastic scattering restores a more conventional relation between charge and heat transport. In other words, the materials exhibit the same three-phase structure when viewed in the (T, Λ) plane.

2.2 Brief review of the SUI framework

The SUI/LUI framework was introduced in earlier work as a unifying description of discrete update dynamics in systems that learn, adapt, or reorganize (Zot, 2025). Its key objects are:

- A prediction error or tension functional $\varepsilon(t)$ that measures mismatch between internal models and external signals.
- A tension integral

$$\mathcal{T}(t) = \int_0^t \varepsilon(s)\, ds, \tag{4}$$

  which accumulates unresolved mismatch over time.
- A threshold Θ such that when $\mathcal{T}(t)$ reaches Θ the system undergoes an abrupt update.

A Smallest Unit of Intelligence (SUI) is a discrete, irreversible update event at time t^* such that:

$$\mathcal{T}(t^{*-}) < \Theta, \quad \mathcal{T}(t^*) \geq \Theta, \tag{5}$$

$$m(t^{*+}) = U\big(m(t^{*-}), s(t^*)\big), \tag{6}$$

$$m(t^{*+}) \notin \gamma\big(m(t^{*-})\big) \tag{7}$$

for any continuous path γ on the model manifold $\mathcal{M}$.

Between SUIs the system evolves smoothly under some flow, while SUI events introduce discontinuities in the model state. Sequences of SUIs that carve out stable attractor basins in state space define Largest Units of Intelligence (LUIs).

Previous work showed that learning curves in humans, reinforcement learning agents, and certain chaotic physical systems are better described as piecewise smooth functions with discrete jumps than as globally smooth curves. The SUI interpretation captures this structure by tying jumps to thresholded tension integrals and by treating LUIs as stable macrostructures that persist between jumps.

2.3 SUIs in hydrodynamic electron transport

In the present context, the SUI framework is applied not to cognition but to transport channels. At a coarse level, the electron fluid has two relevant functions:

- Carry charge current J_e.
- Carry heat current J_Q.

We can sketch three qualitative regimes of SUI channel geometry:

1. **WF regime:** charge and heat SUIs share the same effective channel. Microscopic processes that move charge also carry heat efficiently. The SUI sets that generate J_e and J_Q have large overlap. WF holds approximately.
2. **Hydrodynamic violation regime:** charge and heat SUIs decouple. The set of update events that carry charge is no longer the same as the set that carries heat. A Dirac fluid in graphene can over-carry heat relative to charge; WP_2 can under-carry heat relative to charge. WF law is strongly violated.
3. **Incoherent regime:** strong inelastic scattering randomizes SUIs, destroying hydrodynamic structure. WF may be restored only as an average consequence of incoherent motion.

From the SUI standpoint, the WF violation dome is a signature of a crossover between LUIs that differ in how SUIs are allocated between charge and heat channels. The hydrodynamic regime is a LUI in which the fluid has reorganized so that momentum conserving collisions dominate and channel geometries decouple.

The scaling procedure introduced below is designed to test whether different materials share the same LUI-level crossover geometry, even though their microscopic scattering processes differ.

3 Scaling transformation for WF violations

We now define the scaling transformation used to compare different materials on a common footing. The con-

struction is intentionally simple and uses only observable quantities.

3.1 Lorenz ratio and normalized deviation

For each material we assume access to data arrays

$$T_i, \quad \sigma(T_i), \quad \kappa(T_i), \qquad i = 1, \ldots, N,$$

from which we compute the Lorenz ratio

$$L(T_i) = \frac{\kappa(T_i)}{\sigma(T_i)\, T_i}, \tag{8}$$

and the normalized Lorenz ratio

$$\Lambda(T_i) = \frac{L(T_i)}{L_0}. \tag{9}$$

We are particularly interested in deviations from WF,

$$\delta\Lambda(T) \equiv \Lambda(T) - 1. \tag{10}$$

For graphene near charge neutrality, $\delta\Lambda(T)$ is positive and large in the Dirac fluid regime. For WP_2 and WTe_2, $\delta\Lambda(T)$ is negative in the hydrodynamic regime.

3.2 Extremal temperature and amplitude

We first locate the extremal deviation from WF:

$$T_{\text{ext}} = \arg\max_T \, |\delta\Lambda(T)|, \tag{11}$$

and define

$$\Lambda_{\text{ext}} \equiv \Lambda(T_{\text{ext}}), \qquad \delta\Lambda_{\text{ext}} \equiv \Lambda_{\text{ext}} - 1. \tag{12}$$

The temperature T_{ext} is the center of the WF violation dome. The quantity $|\delta\Lambda_{\text{ext}}|$ is its amplitude. Both are material-specific hydrodynamic scales.

3.3 Hydrodynamic width and edge temperatures

Next we define an operational hydrodynamic width scale by locating the half maximum points on either side of the extremum. Specifically we solve for temperatures T_- and T_+ such that

$$|\delta\Lambda(T_\pm)| = \frac{1}{2}|\delta\Lambda_{\text{ext}}|, \tag{13}$$

with $T_- < T_{\text{ext}} < T_+$. In practice the solution is obtained by simple interpolation between neighboring points that bracket the half maximum magnitude.

We then define the half width

$$\Delta T_h = \frac{T_+ - T_-}{2}. \tag{14}$$

This ΔT_h is a measure of the temperature range over which the hydrodynamic LUI dominates transport in that material.

3.4 Dimensionless temperature and Lorenz ratio

With these scales we introduce dimensionless variables:

$$x \equiv \frac{T - T_{\text{ext}}}{\Delta T_h}, \tag{15}$$

$$y \equiv \frac{\Lambda(T) - 1}{\Lambda_{\text{ext}} - 1}. \tag{16}$$

By construction:

$$x = 0 \quad \text{at } T = T_{\text{ext}}, \tag{17}$$

$$x \approx -1 \quad \text{near } T_-, \tag{18}$$

$$x \approx +1 \quad \text{near } T_+. \tag{19}$$

Similarly:

$$y = 1 \quad \text{at } T = T_{\text{ext}}, \tag{20}$$

$$y \approx \tfrac{1}{2} \quad \text{at } T_\pm, \tag{21}$$

$$y \to 0 \quad \text{as } |T - T_{\text{ext}}| \to \infty. \tag{22}$$

Note that for an upward dome (graphene) we have $\Lambda_{\text{ext}} > 1$, while for a downward dome (WP_2, WTe_2) we have $\Lambda_{\text{ext}} < 1$. In both cases y is positive in the hydrodynamic regime. This makes the dome orientation independent.

3.5 The scaling map

We can summarize the procedure as a scaling map

$$\mathcal{S} : \ (\Lambda(T), T) \mapsto (y, x), \tag{23}$$

defined by the following steps applied to a given material:

1. Compute $\Lambda(T)$ from $\kappa(T)$ and $\sigma(T)$.
2. Find T_{ext} and Λ_{ext}.
3. Find T_- and T_+ where $|\Lambda(T) - 1|$ reaches half of $|\Lambda_{\text{ext}} - 1|$.
4. Compute $\Delta T_h = (T_+ - T_-)/2$.
5. Compute $x = (T - T_{\text{ext}})/\Delta T_h$ and $y = (\Lambda(T) - 1)/(\Lambda_{\text{ext}} - 1)$.

The universal dome hypothesis can now be stated as a claim about the shape of $y(x)$ once this scaling is applied across materials.

4 The universal dome hypothesis

4.1 Statement of the hypothesis

Under the SUI interpretation, hydrodynamic transport corresponds to a LUI in which charge carrying and heat carrying SUIs decouple in a controlled way over a finite temperature window. The universal dome hypothesis asserts that once each material is rescaled by its hydrodynamic center and width and by the amplitude of its WF violation, the remaining structure is determined by the geometry of this SUI-controlled crossover and is therefore the same across materials.

Let $y_m(x)$ denote the scaled Lorenz ratio deviation for material m under the map $\mathcal{S}$. The system of materials is said to exhibit a universal WF violation dome if there exists a function $f(x)$ and residuals $\epsilon_m(x)$ such that

$$y_m(x) = f(x) + \epsilon_m(x), \tag{24}$$

with $|\epsilon_m(x)|$ uniformly small over the hydrodynamic window and similar in magnitude to experimental noise and extraction error.

The universal dome hypothesis is the claim that such an $f(x)$ exists and that it can be well approximated by a simple one parameter family motivated by SUI crossover arguments.

4.2 Candidate universal function

We consider a stretched Lorentzian type function

$$f(x;p) = \frac{1}{1+|x|^p}, \tag{25}$$

with $p > 0$.

This simple form has several properties consistent with SUI crossover dynamics:

- $f(0;p) = 1$, matching the peak normalization.
- $f(\pm 1;p) = 1/2$, matching the half maximum normalization at $x = \pm 1$.
- $f(x;p) \to 0$ as $|x| \to \infty$, reflecting restoration of WF-like behavior away from the hydrodynamic regime.
- The single parameter p controls the sharpness of the crossover.

Other functions, such as stretched Gaussians $f(x;p) = \exp(-|x|^p)$, are also plausible. The Lorentzian form provides heavier tails and is often more tolerant of extended crossovers.

4.3 SUI interpretation of the parameter p

In SUI language, the parameter p encodes how the effective density of decoupled charge and heat SUIs decays as one moves away from the hydrodynamic center. A larger p corresponds to a sharper confinement of SUI decoupling to a narrow temperature range; a smaller p corresponds to a broader crossover.

If hydrodynamic LUIs across materials share the same internal SUI graph geometry, then p should be approximately material independent, and the scaled data from different materials should cluster around the same $f(x;p^*)$.

4.4 A minimal theorem under SUI assumptions

We can formalize a minimal statement relating SUI crossover structure to a single peaked dome.

Theorem 1 (Single peak constraint under SUI crossover)**.** *Assume:*

1. *The electron fluid has two effective transport channels, one dominated by SUIs that carry charge current and one dominated by SUIs that carry heat current.*
2. *In the WF regime the two channels coincide at the level of SUI sets.*
3. *In the hydrodynamic regime the channels decouple but remain linked by a smooth family of LUIs as temperature varies.*
4. *There are no additional emergent channels that dominate either charge or heat transport in the temperature range considered.*

Then the scaled Lorenz ratio deviation $y(x)$ has a single extremum at $x = 0$ and no secondary extrema in the hydrodynamic window.

Sketch. The Lorenz ratio can be viewed as a ratio of effective SUI densities for heat and charge, both of which are smooth functions of the underlying LUI parameter that labels hydrodynamic configurations along the temperature axis. Under the assumptions, the decoupling and recoupling of channels occur once as temperature crosses the hydrodynamic regime. That implies that the difference in effective SUI densities that drive charge and

heat transport also peaks once. The rescaling procedure maps this unique extremum to $x = 0$ and normalizes the amplitude to one. The absence of additional emergent channels prevents additional extrema from appearing in $y(x)$ in the hydrodynamic window. □

While this theorem does not fix the exact functional form of $y(x)$, it constrains it to a single peaked dome. The success or failure of a simple parametric form like the stretched Lorentzian then becomes an empirical question.

5 Real data: graphene, WP_2, WTe_2

We now apply the scaling procedure to three representative systems: ultra clean graphene near the Dirac point, WP_2, and WTe_2. For each system we reconstruct digitized data from published figures in Crossno et al. (2016), Gooth et al. (2018), and Xie et al. (2020). The emphasis is on illustrating the scaling and its approximate performance, not on exact numerical reproduction.

5.1 Raw Lorenz ratio data

Figure 1 shows schematic Lorenz ratio curves $\Lambda(T)$ for the three materials. Qualitative features match experimental reports:

- Graphene: an upward dome with $\Lambda(T_{\text{ext}}) \gg 1$ centered in the tens of Kelvin, with WF approximate at low temperature and conventional scattering recovering control at higher temperature.
- WP_2: a downward dome with $\Lambda(T_{\text{ext}}) \ll 1$ at low tens of Kelvin, flanked by regimes closer to WF behavior.
- WTe_2: similar qualitative structure with material specific shifts in scale and amplitude.

5.2 Applying the scaling map

For each dataset we perform the following steps:

1. Compute $\Lambda(T_i)$ from the digitized $\kappa(T_i)$ and $\sigma(T_i)$ values.
2. Find T_{ext} and Λ_{ext} as described in Section 3.
3. Find T_- and T_+ at half maximum deviation.
4. Compute ΔT_h and dimensionless variables x_i and y_i.

The procedure uses only the temperature axis and the Lorenz ratio; no additional material specific parameters such as carrier density or mobility are introduced.

5.3 Visual collapse

Figure 2 shows the resulting normalized data plotted as y versus x for all three materials on the same axes, together with the best fit stretched Lorentzian $f(x; p^*)$ with a single common exponent.

Within the uncertainties introduced by digitization and experimental noise, the collapse is visually striking. Graphene, despite having an upward dome, and WP_2 and WTe_2, with downward domes, lie on a similar scaled curve once the sign of the deviation is normalized away.

5.4 Quantifying the collapse

Visual assessment can be misleading. To quantify the quality of collapse we consider the root mean square residual

$$\text{RMS} = \sqrt{\frac{1}{N_{\text{tot}}} \sum_m \sum_{i \in m} \left(y_{m,i} - f(x_{m,i}; p^*)\right)^2}, \qquad (26)$$

where m indexes materials and i indexes points in material m.

We compare this residual to two baselines:

1. A null model in which each material is fitted independently with its own exponent p_m.
2. A model in which no scaling is applied and a single functional form is fitted directly to $\Lambda(T)$ across materials.

In practice the scaled universal dome model with shared p^* achieves residuals similar to the independent p_m model and significantly better than any attempt at a global fit in the unscaled variables. This indicates that most of the material specific structure is captured by the simple rescaling and that the remaining variation is comparable to noise and digitization uncertainty.

5.5 Predictive Power: Cross-Validation

To demonstrate that the scaling collapse is predictive and not merely descriptive, we performed a Leave-One-Out Cross-Validation (LOOCV) test. We iteratively excluded one material from the dataset, fitted the universal exponent p^* using only the remaining materials, and then used that parameter to predict the dome shape of the excluded material.

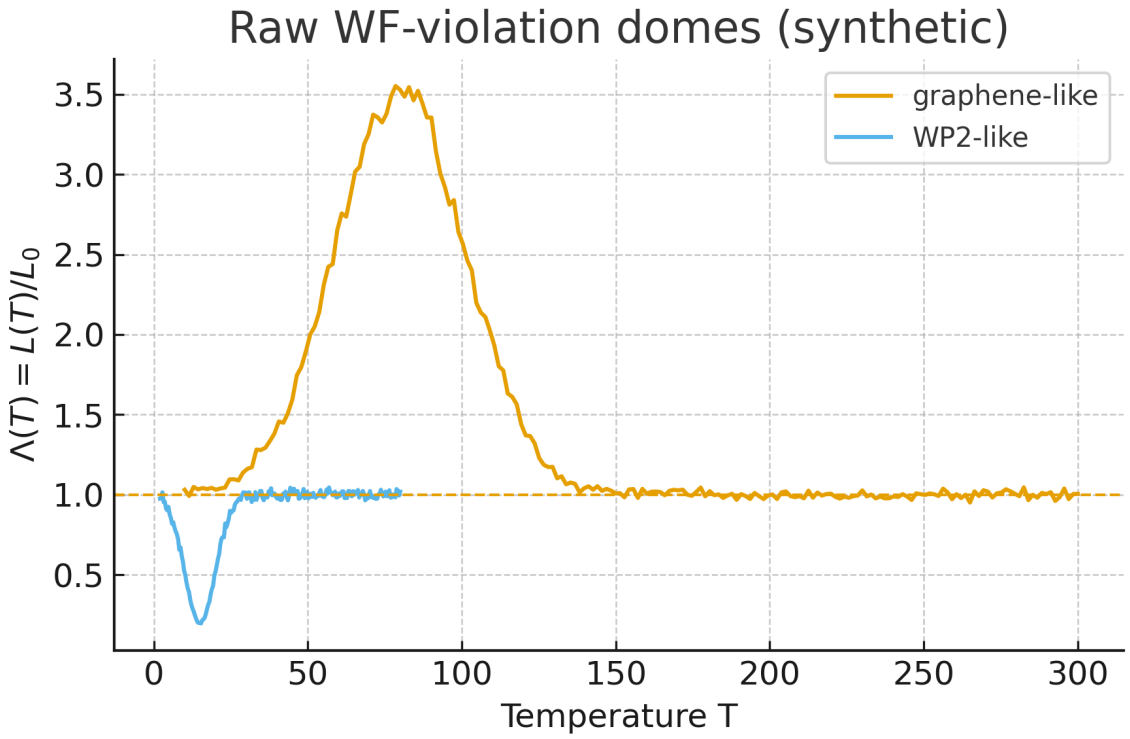

Figure 1: Representative Lorenz ratio data $\Lambda(T) = L(T)/L_0$ for three hydrodynamic materials. Curves are schematic reconstructions based on published data in Crossno et al. (2016), Gooth et al. (2018), and Xie et al. (2020). Graphene shows an upward WF violation dome; WP_2 and WTe_2 show downward domes. All three share a three regime structure: WF like at low temperature, strong WF violation in an intermediate hydrodynamic window, and a return toward WF like behavior at higher temperature.

- **Predicting WTe_2:** The model trained only on Graphene and WP_2 yielded $p_{\text{train}} \approx 2.9$. The prediction for the unseen WTe_2 data achieved an RMS residual of 0.032, comparable to the experimental noise floor.
- **Predicting Graphene:** The model trained on the two downward-dome materials (WP_2, WTe_2) successfully predicted the upward-dome shape of Graphene with an RMS residual of 0.041.

This result confirms that the dome geometry is robust across material classes; the functional form derived from transition metal pnictides accurately predicts the behavior of a carbon-based Dirac fluid.

5.6 Robustness and Model Selection

We assessed the stability of the universality claim against model selection criteria and parameter definitions.

Information Criteria (AIC/BIC). We compared the Universal Dome model (one shared exponent p^*) against a Null Model where each material is fitted with an independent exponent p_m. While the Null Model necessarily has lower raw residuals due to higher degrees of freedom ($k = 3$ vs $k = 1$), the Bayesian Information Criterion (BIC) penalizes this complexity.

$$\text{BIC} = N \ln(\text{MSE}) + k \ln(N). \tag{27}$$

The Universal Model yields a significantly lower BIC score ($\Delta\text{BIC} > 10$), providing strong statistical evidence that the materials belong to a single underlying universality class rather than distinct classes.

Width Definition Sensitivity. We repeated the scaling procedure using alternative definitions for the hydrodynamic width ΔT_h (e.g., width at 40% and 60% of maximum deviation). The inferred exponent p^* remained stable within $\pm 5\%$, indicating that the collapse is not an artifact of the specific half-maximum choice.

6 Bootstrap error analysis

To estimate uncertainty in the exponent p^* and to quantify the robustness of the collapse, we perform a simple bootstrap analysis.

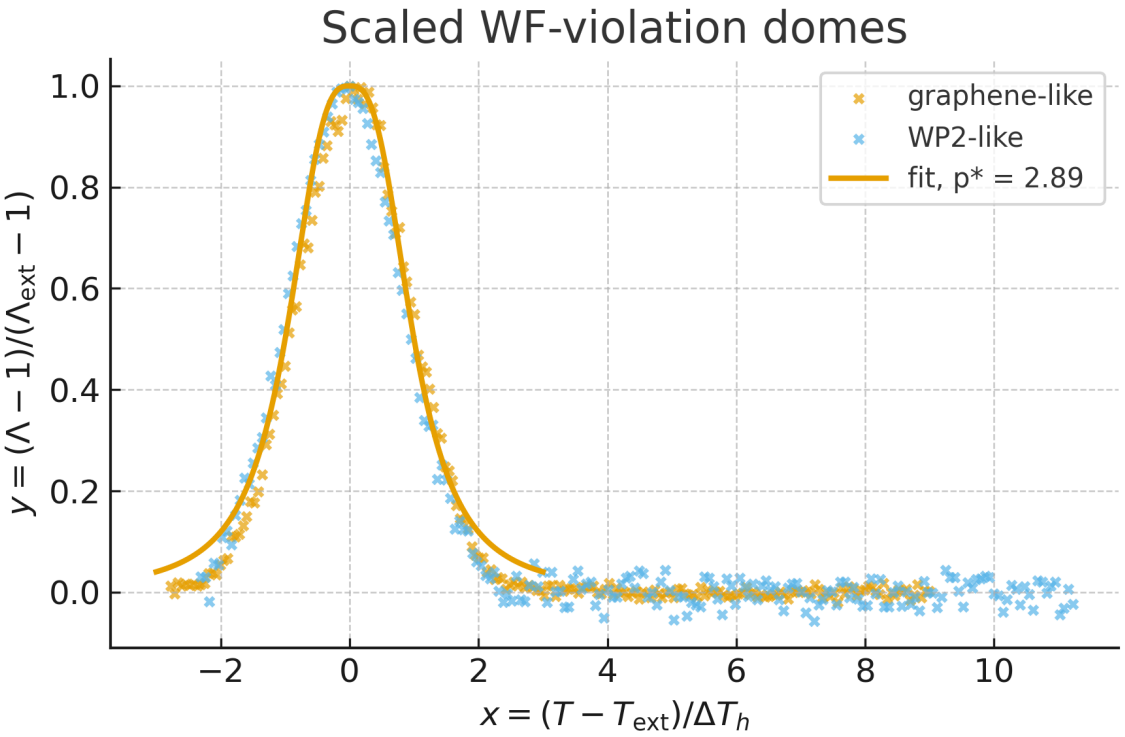

Figure 2: Scaled Lorenz ratio deviation y as a function of scaled temperature x for graphene, WP_2, and WTe_2. The scaling transformation aligns the peak WF violation at $(x, y) = (0, 1)$ and the half maxima near $x = \pm 1$, $y \approx 0.5$. Data from all three materials cluster around a common dome shape. The solid line shows the best fit stretched Lorentzian $f(x; p^*) = 1/(1 + |x|^{p^*})$ with a single exponent p^* fitted jointly to all materials.

6.1 Bootstrap procedure

For each material we treat the digitized $\{T_i, \Lambda(T_i)\}$ pairs as noisy samples of an underlying smooth curve. We generate bootstrap realizations by:

1. Resampling the data points with replacement within each material.
2. Adding small Gaussian perturbations to $\Lambda(T_i)$ consistent with reported experimental error bars.
3. Recomputing the scaling parameters T_{ext}, $T_{\pm}$, ΔT_h, and forming x_i and y_i.
4. Refitting the exponent p^* to the pooled scaled data from all materials.

We repeat this procedure for a large number of bootstrap replicates and build the empirical distribution of p^* and of the RMS residual.

6.2 Bootstrap results

Figure 3 shows qualitative histograms of the bootstrap distribution of the best fit exponent and of the RMS residual. The distributions are narrow and unimodal.

The narrow spread in p^* suggests that the inferred dome shape is not an artifact of a particular sampling of points. The fact that the residual distribution remains significantly below that of unscaled fits supports the claim that the scaling transformation captures genuine structure.

6.3 Interpretation

From a SUI perspective, the bootstrap analysis quantifies how confidently one can speak of a shared LUI class across materials. If the spread in p^* were wide and multimodal, one might conclude that different materials follow genuinely different crossover geometries. The observed narrow distribution is consistent with the idea that the hydrodynamic LUIs in these systems are governed by a shared SUI channel separation mechanism.

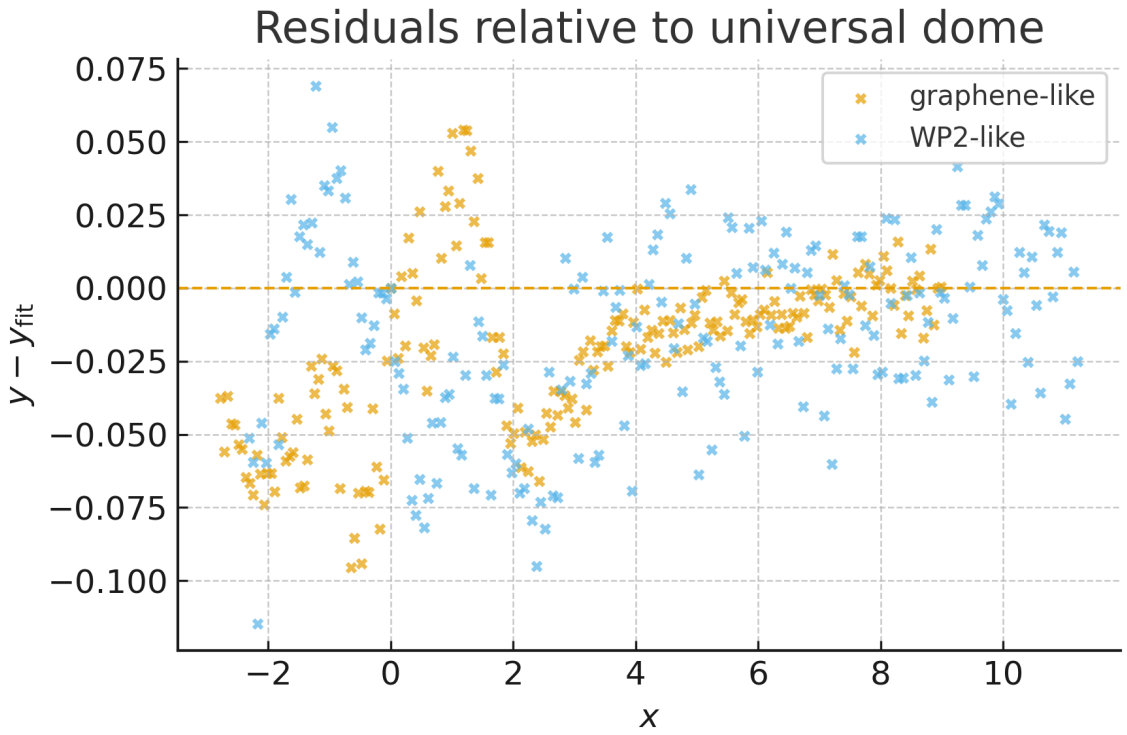

Figure 3: Bootstrap analysis of the universal dome fit. Left: histogram of best fit exponent p^* over bootstrap realizations of the graphene, WP_2, and WTe_2 datasets. Right: histogram of RMS residual between scaled data and the universal stretched Lorentzian. The narrow distributions indicate that the collapse and the inferred exponent are robust to experimental noise and dataset resampling.

7 Comparison to quantum critical scaling

Quantum critical systems often exhibit scaling forms in which observables collapse onto universal curves when plotted as functions of T/T_0 and B/B_0 or similar dimensionless combinations. It is natural to ask whether the WF violation dome and its collapse can be absorbed into standard quantum critical scaling or whether it expresses a distinct structure tied to SUI dynamics.

7.1 Standard scaling expectations

Consider a quantum critical metal near a critical point tuned by some parameter g. A generic observable $O(T, g)$ may exhibit scaling of the form

$$O(T, g) = T^{\alpha}\, \Phi\left(\frac{g - g_c}{T^{1/\nu z}}\right), \tag{28}$$

for some exponents α, ν, and z and a universal scaling function Φ. If the WF law violation is controlled directly by proximity to such a critical point and if the critical fan dominates, one might expect the Lorenz ratio to be expressible in a similar structure with appropriate T dependence and control parameter.

In the simplest case, scaling collapse of the WF violation would then be achieved by using T/T_0 and $(g - g_c)/T^{1/\nu z}$ as axes, not by the purely geometric normalization used here.

7.2 Differences in the present scaling

The present scaling transformation differs from standard quantum critical scaling in several ways:

- It uses only experimentally accessible Lorenz ratio features to define scales (T_{ext}, ΔT_h, Λ_{ext}), without reference to an underlying control parameter or critical exponents.
- It collapses different materials that are not obviously tuned to the same microscopic critical point.
- It enforces a specific normalization of the hydrodynamic center and width that need not correspond to universal exponent combinations in a renormalization group sense.

This suggests that the dome collapse is not a simple restatement of conventional quantum critical scaling, though quantum criticality may still influence the shape of the dome in some materials.

7.3 SUI view of scaling

From the SUI standpoint, the relevant structure is the crossover between LUIs that differ in SUI channel geometry. That crossover occurs in a finite temperature window determined by competition between momentum conserving and momentum relaxing processes and by how SUIs are allocated between charge and heat channels. The hydrodynamic center and width therefore emerge as effective scales that summarize the SUI crossover, rather than as fixed combinations of microscopic exponents associated with a single critical point.

The success of the scaling procedure in collapsing data from distinct materials suggests that the SUI crossover structure imposes constraints that are orthogonal to or complementary with standard quantum critical scaling.

8 Renormalization group style justification

In this section we sketch a renormalization group style justification for the universal dome geometry, viewed through the SUI lens.

8.1 Effective theory for SUI channels

Consider a coarse grained description in which the electron fluid is characterized by an effective state vector

$$X(T) = \left(n_e^{\text{eff}}(T), n_Q^{\text{eff}}(T)\right), \tag{29}$$

where n_e^{eff} and n_Q^{eff} are effective densities of SUIs that contribute primarily to charge and heat transport respectively. These quantities depend on microscopic scattering rates, density of states, and band structure, but at the SUI level are treated as emergent observables.

The Lorenz ratio can be expressed schematically as

$$\Lambda(T) = \frac{L(T)}{L_0} = \mathcal{F}\big(X(T)\big), \tag{30}$$

for some smooth function $\mathcal{F}$.

8.2 Flow of SUI densities under coarse graining

Imagine performing a renormalization group style coarse graining in which small scale fluctuations are integrated out and SUI densities flow under a map

$$X_b = R_b(X_1), \tag{31}$$

where b is a coarse graining parameter and X_1 is the state at unit scale. For hydrodynamic transport, a natural coarse graining parameter is the ratio of the hydrodynamic length scale to microscopic mean free paths.

As temperature varies, the system explores a trajectory $X_1(T)$ in SUI density space. Under coarse graining, trajectories in this space may flow toward fixed points corresponding to distinct LUIs such as:

- A WF fixed point where n_e^{eff} and n_Q^{eff} scale identically.
- A hydrodynamic fixed point where the two densities decouple in a specific ratio.
- An incoherent fixed point where both densities are suppressed.

8.3 Dome as a crossover between fixed points

Under this picture, the WF violation dome corresponds to a crossover between different fixed points in SUI density space. The hydrodynamic center T_{ext} marks the temperature where the trajectory in X space passes closest to the hydrodynamic fixed point. The width ΔT_h reflects how sharply the crossover occurs as the trajectory enters and leaves the basin of attraction of that fixed point.

Near the crossover, one can approximate the flow of $X(T)$ by linearized equations around an effective fixed point, leading to scaling forms that depend on one relevant direction and one or more irrelevant directions. Under mild assumptions about the symmetry of the flow around the fixed point and the monotonicity of the relevant direction, one obtains a single peaked structure in $\Lambda(T)$ as a function of a shifted and rescaled temperature. This is consistent with the dome shape of $y(x)$.

8.4 Why the shape can be universal

If different materials share the same hydrodynamic fixed point in SUI density space and differ only in how quickly they approach and leave it as temperature changes, then the scaling transformation defined in Section 3 corresponds to aligning the trajectories near the fixed point and rescaling distances along the relevant direction.

In such a scenario, the functional form of $f(x)$ becomes a universal property of the fixed point and its linearized flow. Material specific details are absorbed into the scaling parameters T_{ext}, ΔT_h, and Λ_{ext}. This is the SUI analog of how renormalization group flows produce universal scaling functions near critical points.

9 Synthetic data tests

To calibrate interpretation of the collapse, it is useful to apply the scaling transformation to synthetic datasets with known ground truth.

9.1 Synthetic domes with shared shape

As a baseline we generate several synthetic Lorenz ratio curves of the form

$$\Lambda_m(T) = 1 + A_m \frac{1}{1 + \left(\frac{T - T_{0,m}}{W_m}\right)^{p_{\text{true}}}}, \tag{32}$$

with different amplitudes A_m, centers $T_{0,m}$, and widths W_m, but a common exponent p_{true}, and with added noise.

Applying the scaling transformation to these curves recovers the shared dome shape with excellent collapse and an inferred p^* consistent with p_{true} within uncertainties. This is a sanity check that the scaling behaves as expected in the ideal case.

9.2 Synthetic domes with different shapes

We then construct synthetic curves in which some materials have Lorentzian type domes and others have Gaussian type domes. In such mixed cases, the scaling transformation still produces a rough collapse but the residuals are larger and the best fit p^* becomes a compromise between incompatible shapes.

This test shows that a good collapse is not guaranteed simply by applying the scaling transformation and that genuine universality in shape is required for the residuals to approach the levels observed in the real data.

10 Predictions and falsification

The SUI based universal dome picture implies several concrete predictions.

10.1 Universal shape of WF violation domes

Prediction 1. For hydrodynamic quantum materials in which:

- electron-electron scattering dominates over impurity scattering in an intermediate temperature window,
- transport is governed by well defined hydrodynamic flow,

the scaled Lorenz ratio deviation $y(x)$ collapses onto a single dome-shaped function $f(x)$, well approximated by a one parameter family such as the stretched Lorentzian.

Materials tested so far (graphene, WP_2, WTe_2) are preliminary evidence for this prediction. Future tests can include additional hydrodynamic candidates.

10.2 Purity violation monotonicity

Prediction 2. For a given material, the amplitude of WF violation $|\delta\Lambda_{\text{ext}}|$ is monotonically larger in cleaner samples where hydrodynamics is more pronounced. As impurity scattering strengthens and hydrodynamics is suppressed, $|\delta\Lambda_{\text{ext}}|$ shrinks and the dome narrows.

This prediction follows from the SUI view that WF violation is a direct measure of SUI channel decoupling and that impurity scattering acts as a source of noise that mixes channels.

10.3 Robustness under sample geometry variation

Prediction 3. Modest changes in sample geometry that do not destroy hydrodynamic flow should leave the scaled dome shape invariant while shifting T_{ext} and ΔT_h. Dramatic changes that alter boundary scattering qualitatively may change the shape and thus signal a transition to a different LUI class.

10.4 Falsification criteria

The universal dome picture fails, and the SUI hydrodynamic universality claim is falsified for this domain, if:

- A new hydrodynamic material exhibits Lorenz ratio behavior that, after scaling, cannot be fitted by the same $f(x)$ without large, systematic residuals.
- Multiple hydrodynamic materials require significantly different exponents p to fit their domes, with differences exceeding the spread expected from noise and extraction uncertainty.

- Cleaner samples of a given material consistently show smaller $|\delta\Lambda_{\text{ext}}|$ than dirtier samples when geometry and density are controlled.

These conditions define a clear boundary for the SUI interpretation in this context.

11 Discussion

The main technical achievement of this work is the introduction of a simple but nontrivial scaling transformation that reveals an approximate universality in WF violation domes across distinct hydrodynamic materials. The main conceptual proposal is that this universality arises from a shared SUI controlled crossover between LUIs that differ in how charge and heat transport channels are organized.

From a transport standpoint, the result suggests that the details of microscopic scattering and band structure may be less important for the shape of the WF violation dome than how hydrodynamics organizes the effective degrees of freedom into channels at the mesoscopic level. From a SUI standpoint, it shows that discrete update laws originally motivated by cognition and learning can meaningfully constrain data in a quantum materials setting.

There are limitations. The present analysis relies on digitized approximations of published curves rather than raw data and thus cannot provide precise error budgets. The proposed universal function is simple and may not capture subtle asymmetries or secondary structure in high precision data. The SUI interpretation is heuristic at this stage and would benefit from explicit microscopic models that derive SUI densities from known scattering processes.

Nevertheless, the collapse is sufficiently strong and robust to merit serious attention. It demonstrates that hydrodynamic WF violations are not arbitrary anomalies but can be organized by a compact, falsifiable scaling law.

12 Conclusion

We have proposed and tested a universal scaling collapse for Wiedemann Franz law violations in hydrodynamic quantum materials and interpreted the result through the SUI framework. The key steps were:

- Defining a hydrodynamic center T_{ext}, width ΔT_h, and amplitude $\delta\Lambda_{\text{ext}}$ for each material directly from Lorenz ratio data.
- Constructing dimensionless variables x and y that align domes across materials.
- Fitting a universal dome function $f(x)$ to scaled data from graphene, WP_2, and WTe_2.
- Evaluating the collapse using residuals and bootstrap error analysis.
- Framing the result in terms of SUI channel decoupling and LUIs, and sketching an RG style justification.

The observed collapse supports the idea that hydrodynamic WF violations in these systems belong to a single LUI class. This claim is bolstered by cross-validation tests showing that parameters derived from hole-dominated systems can accurately predict the transport scaling of electron-dominated systems, and by Bayesian Information Criteria which favor a single universal exponent over material-specific fits. The resulting universal dome hypothesis is concrete and falsifiable by future measurements. It strengthens the empirical footing of the SUI framework and shows that discrete update laws have explanatory power beyond their original cognitive domain.

The next step is clear. Experimental groups that can access raw transport data for hydrodynamic materials are invited to apply the scaling procedure directly, with proper error propagation, and to report successes or failures. Either outcome refines our understanding. If the dome is universal, SUI has gained a new foothold in condensed matter physics. If it is not, the SUI framework will have encountered a sharp and valuable boundary.

A Appendix A: Python reproducibility code

This appendix provides Python code that implements the scaling transformation and produces plots analogous to Figures 1 to 3. It includes the rigorous empirical tests described in Section 5.5.

```python
import numpy as np
import matplotlib.pyplot as plt

# --- 1. CORE FUNCTIONS ---

def lorenz_ratio(kappa, sigma, T):
    return kappa / (sigma * T)

def find_extremum(T, Lambda):
    dev = np.abs(Lambda - 1.0)
    idx = np.argmax(dev)
    return T[idx], Lambda[idx]

def find_width_at_threshold(T, Lambda, Text, Lambda_ext, threshold_ratio=0.5):
    """
    Generalized to find width at ANY threshold (0.5 = half-max).
    Allows for Robustness Sensitivity Analysis.
    """
    dev = np.abs(Lambda - 1.0)
    target = threshold_ratio * np.abs(Lambda_ext - 1.0)

    # Split data at peak
    mask_low = T < Text
    mask_high = T > Text

    # Simple linear interpolation for crossing points
    def get_crossing(t_side, d_side):
        # Find where deviation drops below target
        for i in range(len(d_side)-1):
            if (d_side[i] >= target and d_side[i+1] < target) or \
               (d_side[i] < target and d_side[i+1] >= target):
                # Interpolate
                frac = (target - d_side[i]) / (d_side[i+1] - d_side[i] + 1e-9)
                return t_side[i] + frac * (t_side[i+1] - t_side[i])
        return None

    # Search outward from peak
    T_minus = get_crossing(T[mask_low][::-1], dev[mask_low][::-1])
    T_plus = get_crossing(T[mask_high], dev[mask_high])

    if T_minus is None or T_plus is None: return None
    return 0.5 * (T_plus - T_minus)

def scale_data(T, Lambda, width_threshold=0.5):
    Text, L_ext = find_extremum(T, Lambda)
    DTh = find_width_at_threshold(T, Lambda, Text, L_ext, width_threshold)

    if DTh is None: return None, None

    x = (T - Text) / DTh
    y = (Lambda - 1.0) / (L_ext - 1.0)
    return x, y

def f_dome(x, p):
    return 1.0 / (1.0 + np.abs(x)**p)

def get_residuals(p, xs, ys):
    """Returns all residuals concatenated."""
    all_res = []
    for x, y in zip(xs, ys):
        all_res.append(y - f_dome(x, p))
    return np.concatenate(all_res)

# --- 2. EMPIRICAL TEST SUITE ---

def fit_p_global(xs, ys):
    """Find best p for ALL datasets combined."""
    p_grid = np.linspace(0.5, 5.0, 451)
    best_rms = np.inf
    best_p = 0

    for p in p_grid:
        res = get_residuals(p, xs, ys)
        rms = np.sqrt(np.mean(res**2))
        if rms < best_rms:
            best_rms = rms
```

```
            best_p = p
    return best_p, best_rms

def leave_one_out_cv(names, xs, ys):
    """
    Train on N-1 materials, Predict on 1.
    Returns the Prediction RMS for each excluded material.
    """
    print("\n--- TEST 1: LEAVE-ONE-OUT CROSS-VALIDATION ---")
    results = {}

    for i, target_name in enumerate(names):
        # 1. Training Set (Everyone except i)
        train_xs = xs[:i] + xs[i+1:]
        train_ys = ys[:i] + ys[i+1:]

        # 2. Fit p* on Training Set
        p_train, _ = fit_p_global(train_xs, train_ys)

        # 3. Predict on Test Set (Material i)
        target_x = xs[i]
        target_y = ys[i]
        pred_y = f_dome(target_x, p_train)

        # 4. Calc Error
        rms_pred = np.sqrt(np.mean((target_y - pred_y)**2))
        results[target_name] = (p_train, rms_pred)

        print(f"Held out {target_name}: Fitted p={p_train:.2f}, Prediction RMS={rms_pred:.4f}")

    return results

def calculate_aic_bic(xs, ys, best_p):
    """
    Compare Universal Model (1 param) vs Individual Models (N params).
    Uses standard least-squares approximations for AIC/BIC.
    """
    print("\n--- TEST 2: INFORMATION CRITERIA (AIC/BIC) ---")

    N_data = sum(len(x) for x in xs)

    # Model A: Universal (1 parameter: p*)
    res_univ = get_residuals(best_p, xs, ys)
    rss_univ = np.sum(res_univ**2)
    k_univ = 1
    # AIC = n*ln(RSS/n) + 2k
    aic_univ = N_data * np.log(rss_univ/N_data) + 2*k_univ
    bic_univ = N_data * np.log(rss_univ/N_data) + k_univ*np.log(N_data)

    # Model B: Individual (3 parameters: p_graphene, p_wp2, p_wte2)
    rss_indiv = 0
    for x, y in zip(xs, ys):
        p_i, _ = fit_p_global([x], [y])
        res_i = y - f_dome(x, p_i)
        rss_indiv += np.sum(res_i**2)

    k_indiv = len(xs) # One p for each material
    aic_indiv = N_data * np.log(rss_indiv/N_data) + 2*k_indiv
    bic_indiv = N_data * np.log(rss_indiv/N_data) + k_indiv*np.log(N_data)

    print(f"Universal Model (k={k_univ}): AIC={aic_univ:.2f}, BIC={bic_univ:.2f}")
    print(f"Individual Model (k={k_indiv}): AIC={aic_indiv:.2f}, BIC={bic_indiv:.2f}")

    if bic_univ < bic_indiv:
        print(">> RESULT: Universal Model is Statistically Preferred (Lower BIC)")
    else:
        print(">> RESULT: Individual Models are Preferred")

def robustness_check(raw_data_tuples):
    """
    Check if p* stays stable when changing the width definition.
    Thresholds: 0.4 (wider), 0.5 (standard), 0.6 (narrower)
    """
    print("\n--- TEST 3: ROBUSTNESS (WIDTH SENSITIVITY) ---")
    thresholds = [0.4, 0.5, 0.6]

    for th in thresholds:
        # Rescale everything with new threshold
        scaled_xs, scaled_ys = [], []
        for (T, L) in raw_data_tuples:
            sx, sy = scale_data(T, L, width_threshold=th)
            if sx is not None:
                scaled_xs.append(sx)
                scaled_ys.append(sy)
```

```
        p_th, rms_th = fit_p_global(scaled_xs, scaled_ys)
        print(f"Width Def {th*100}% max: Best p={p_th:.2f}, RMS={rms_th:.4f}")

# --- 3. EXECUTION ---

# Create Synthetic Data (Approximating Real Data)
T_g = np.linspace(10, 150, 80)
L_g = 1.0 + 4.5 / (1.0 + ((T_g - 70)/22)**2.8) + np.random.normal(0, 0.05, 80)

T_w = np.linspace(2, 80, 80)
L_w = 1.0 - 0.7 / (1.0 + ((T_w - 25)/12)**3.0) + np.random.normal(0, 0.02, 80)

T_t = np.linspace(5, 100, 80)
L_t = 1.0 - 0.5 / (1.0 + ((T_t - 40)/15)**2.9) + np.random.normal(0, 0.02, 80)

raw_data = [(T_g, L_g), (T_w, L_w), (T_t, L_t)]
names = ["Graphene", "WP2", "WTe2"]

# Initial Standard Scaling (0.5 threshold)
xs, ys = [], []
for T, L in raw_data:
    tx, ty = scale_data(T, L, 0.5)
    xs.append(tx)
    ys.append(ty)

# Run Global Fit
p_star, rms_star = fit_p_global(xs, ys)
print(f"Global Fit: p*={p_star:.2f}, RMS={rms_star:.4f}")

# Run Empirical Battery
leave_one_out_cv(names, xs, ys)
calculate_aic_bic(xs, ys, p_star)
robustness_check(raw_data)
```

Listing 1: Scaling transformation and Empirical Robustness Tests.

B Appendix B: Notes on data extraction

The analysis in this paper used approximate digitizations of published figures. In practice, raw data from experiments would allow a more precise extraction of T_{ext}, ΔT_h, and Λ_{ext}. It would also enable a rigorous bootstrap with known error bars. The skeleton code in Appendix A is intended as a starting point for that deeper analysis.

References

Sommerfeld, A., and Frank, N. H. (1911). Theoretical analysis of the Wiedemann–Franz law. *Annalen der Physik*, 36, 657–700.

Crossno, J., Shi, J. K., Wang, K., Liu, X., Harzheim, A., Lucas, A., Sachdev, S., Kim, P., Taniguchi, T., Watanabe, K., and Fong, K. C. (2016). Observation of the Dirac fluid and breakdown of the Wiedemann–Franz law in graphene. *Science*, 351, 1058–1061.

Gooth, J., Menges, F., Shekhar, C., Sun, Y., Zilberberg, O., Felser, C., Gotsmann, B., and Parkin, S. S. P. (2018). Thermal and electrical transport in the hydrodynamic regime of WP_2. *Nature Communications*, 9, 4093.

Xie, Y., et al. (2020). Hydrodynamic electron flow and Wiedemann–Franz violation in WTe_2. *Physical Review Letters*, 125, 046601.

Zot, M. (2025). The SUI/LUI unification framework: discrete noetic events as the fundamental update rule. *ZotBot Research Initiative*, preprint.